ADVANCED FUNCTIONAL MATERIALS
www.afm-journal.de

Temperature Dependence of the Piezophototronic Effect in CdS Nanowires

*Ruomeng Yu, Xingfu Wang, Wenzhuo Wu, Caofeng Pan, Yoshio Bando, Naoki Fukata, Youfan Hu, Wenbo Peng, Yong Ding, and Zhong Lin Wang**

The piezophototronic effect is known as a three-way coupling between piezoelectric polarization, semiconductor property, and optical excitation in piezoelectric semiconductor materials to modify their energy band structures by strain-induced piezoelectric polarization charges, and thus to tune/control their optoelectronic processes of charge carrier generation, separation, recombination, and transport. In this work, the temperature dependence of the piezophototronic effect in wurtzite-structured CdS nanowires is investigated from 77 to 300 K. The piezophototronic effect is enhanced by over 550% under lower temperature due to the increased effective piezoelectric polarization surface/interface charges resulting from the reduced screening effect by decreased mobile charge carriers in CdS nanowires. Optoelectronic performances of CdS nanowires are systematically investigated under various light illuminations, strains, and temperatures. By analyzing the corresponding band diagrams, the piezophototronic effect is found to dominate the transport and separation processes of charge carriers. This study presents in-depth fundamental understanding about the piezophototronic effect and provides guidance for its future applications in optoelectronic devices.

1. Introduction

Wurtzite-structured materials with noncentrosymmetric crystal structures present piezoelectric polarizations under mechanical deformations due to the relative displacements between the centers of positive and negative ions. In piezoelectric semiconductor materials, such as ZnO, CdS, and even monolayer dichalcogenides, the mechanical strain–induced piezoelectric polarization charges created at the vicinity of local interface/junction can modify the band profiles.[1–4] The optoelectronic processes of charge carriers, such as generation, separation, recombination, and/or transport, could therefore be tuned by strain-induced piezoelectric polarization charges, which is the piezophototronic effect.[2] As a three-way coupling among piezoelectric polarization, semiconductor property, and optical excitation, the piezophototronic effect has been extensively investigated and led to both novel fundamental phenomena[5] and unprecedented device characteristics as well as applications[1,6] in various fields, including solar cells,[7] light emitting diodes (LEDs),[8] photodetectors,[9] and logic computations.[10] Promising future and numerous potential applications have been demonstrated for this new emerging effect, however, all of the existing researches are performed at room temperature. Neither the temperature dependence of the piezophototronic effect nor the corresponding performances of the piezophototronic devices under various temperatures have been systematically studied. Considering the complex and unpredictable working environments the devices may experience, it is of great significance to explore the temperature-determined performances of the piezophototronic devices not only for thoroughly understanding the fundamentals of the three-way coupling effect in nanostructures, but also for guiding the design and fabrication of novel optoelectronic devices.

In this work, the temperature dependence of the piezophototronic effect in cadmium sulfide nanowires (CdS NWs) is systematically investigated by varying the temperature from 77 to 300 K. Optoelectronic behaviors of CdS NWs are carefully measured by applying a series of light illuminations and straining conditions at each temperature. Under mechanical strains, the corresponding energy band diagrams indicate that the piezophototronic effect dominates the transport and separation processes of charge carriers by utilizing strain-induced piezoelectric polarization charges at local interface/junction to modulate the energy band structures of CdS NWs. The piezophototronic effect is significantly enhanced by over 550% as lowering the

R. Yu, X. Wang, Dr. W. Wu, W. Peng, Dr. Y. Ding, Prof. Z. L. Wang
School of Materials Science and Engineering
Georgia Institute of Technology
Atlanta, GA 30332-0245, USA
E-mail: zhong.wang@mse.gatech.edu
Prof. C. Pan, Prof. Z. L. Wang
Beijing Institute of Nanoenergy and Nanosystems
Chinese Academy of Sciences
Beijing 100083, P.R. China
Prof. Y. Bando, Prof. N. Fukata
International Center for Materials Nanoarchitectonics
National Institute for Materials Science
1-1 Namiki, Tsukuba 305-0044, Japan
Prof. Y. Hu
Key Laboratory for the Physics and Chemistry of Nanodevices
Department of Electronics
Peking University
Beijing 100871, P.R. China

DOI: 10.1002/adfm.201501986

system temperature, since the effective piezoelectric polarization surface/interface charge density is increased due to the reduced screening effect by decreased mobile charge carrier density in CdS NWs at lower temperature. The conductivity, mobile charge carrier density, effective polarization charge density, and the corresponding changes of Schottky barrier height (SBH) of CdS NWs are calculated based on theoretical simulations at various temperatures. This work explores the temperature dependence and the fundamental working mechanism of the piezophototronic effect, guiding the future design and fabrication of piezophototronic devices for optical communications, human-machine interfacing, health monitoring systems, and implantable surgical instruments.[11]

2. Results and Discussion

2.1. Fundamental Characterizations

CdS NWs used in this work are synthesized through a vapor–liquid–solid (VLS) process described elsewhere.[12] A typical scanning electron microscope (SEM, Hitachi SU8010) image of the as-synthesized CdS NW is shown in **Figure 1**a1, with the diameter of CdS NWs near 300 nm and the length in several hundred micrometers. The corresponding selected area electron diffraction (SAED, Tecnai G2) patterns and high-resolution transmission electron microscope (HRTEM, FEI F30) image are presented in Figure 1a2,a3, respectively, indicating that the single crystalline CdS NWs grow along [0001] direction (*c*-axis) and possess noncentrosymmetric wurtzite structure.[13]

Optoelectronic performances of the CdS NW devices are measured in a micromanipulation cryogenic probe system (Janis, model ST-500-2) as schematically shown in Figure 1b. Using liquid nitrogen as the cryostat, the temperature of the whole system ranges from 77 to 300 K. To maintain reliable thermal equilibrium between the CdS NW and the cryostat, aluminum foil (76 μm in thickness) covered with a layer of Kapton tape (30 μm in thickness) is adopted as the substrate, which features with excellent thermal conductivity, an insulating surface, and satisfactory mechanical flexibility. The thermal expansion coefficients of aluminum and Kapton tape are 23.1×10^{-6} and 20×10^{-6} °C^{-1},[14] respectively. Substrate deformations due to the mismatch of thermal expansion coefficients can therefore be neglected. The device is fabricated by transferring and bonding an individual CdS NW laterally on this substrate with its *c*-axis in the plane of the substrate. Silver paste is applied to fix both ends of the NW, serving as source and drain electrodes to form a metal–semiconductor–metal (M–S–M) structure with two Schottky contacts. By fixing the device at the edge of the cryostat (Figure 1b, upper right corner), mechanical strains are introduced through a micromanipulating probe attached to one of the probing station arms moving in 3D. The values of the externally applied tensile strains are calculated following the method reported previously by Yang et al.[15] A beam of green laser light with wavelength of 532 nm is shined on the device to provide optical stimuli. The electric output signals are measured and collected by computer-controlled program through a GPIB controller; details are found in the Experimental Section.

Two sets of typical *I*–*V* characteristics are presented in Figure 1c,d, showing the temperature and strain response of the

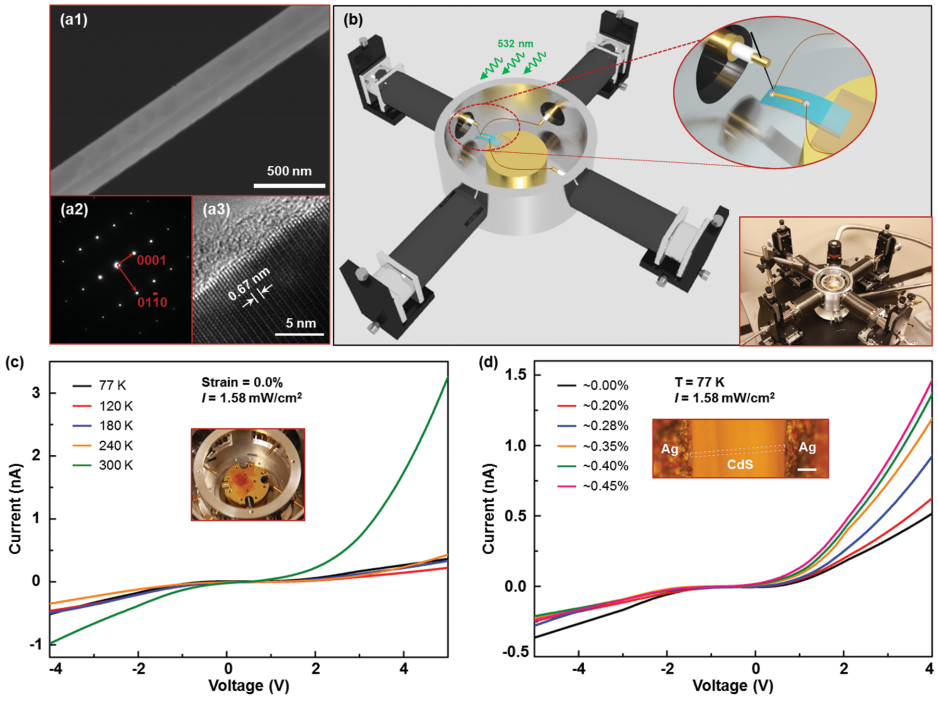

Figure 1. Structure and transport characterizations of CdS NWs. a1) SEM image, a2) SAED pattern, and a3) HRTEM image of the as-synthesized CdS NW. b) Schematic illustration and digital image of the micromanipulation cryogenic probe station system as experimental setups. *I*–*V* characteristics of CdS NW devices under various c) temperatures and d) straining conditions.

Adv. Funct. Mater. **2015**,
DOI: 10.1002/adfm.201501986

CdS NW devices, respectively. Under strain-free condition and green laser illumination with power density of 1.58 mW cm^{-2}, the devices display larger output currents at room temperatures (Figure 1c), indicating that the conductivity of the CdS NWs increases significantly at room temperature compared to that at low temperature. At 77 K, by applying a beam of green laser with power density of 1.58 mW cm^{-2}, the output currents increase at positive biased voltages while decrease at the negative side when increasing the externally applied tensile strains from 0% to 0.45%, as shown in Figure 1d. These observed results represent the typical transport properties of CdS NWs dominated by the piezotronic effect,[4] which leads to asymmetric changes of barrier heights and thus the output currents at two Schottky contacts. An optical image of the as-fabricated CdS NW device is presented as the inset of Figure 1d.

2.2. Current Responses of CdS NW Devices

The output currents response of CdS NW devices to various temperatures and illumination intensities at both positive and negative biased voltages are systematically investigated and summarized in **Figure 2**, under strain-free condition. Figure 2a,b displays the temperature response of CdS NW devices under different illumination conditions at –4 and +5 V biased voltages, respectively. It is obvious that the output currents increase significantly at room temperature compared to those under low temperatures under each illumination intensity for both negative (Figure 2a) and positive (Figure 2b) biased voltages. These results are reasonable since the carrier density of CdS NWs is determined by ionization of shallow level dopants. As decreasing the temperature, the carrier density decreases due to the freeze-out, leading to a decreased conductance and output currents at lower temperature. Furthermore, the conductivity and carrier density of CdS NWs under strain-free condition and green laser illumination (power density = 1.58 mW cm^{-2}) are calculated and plotted as a function of temperature as presented in Figure S1 (Supporting Information), clearly showing smaller conductivity and lower carrier density at lower temperature. These electrical parameters are derived by simulating the transport properties of CdS NWs quantitatively through an M–S–M model,[16,17] details are found in the Supporting Information. By fixing the measurement temperature at 77, 120, 180, 240, and 300 K, the output current responses of CdS NW devices to illumination intensities are presented in Figure 2c (–4 V biased voltage) and 2d (+5 V biased voltage). It is straightforward to observe increased currents under stronger laser illuminations at each temperature.

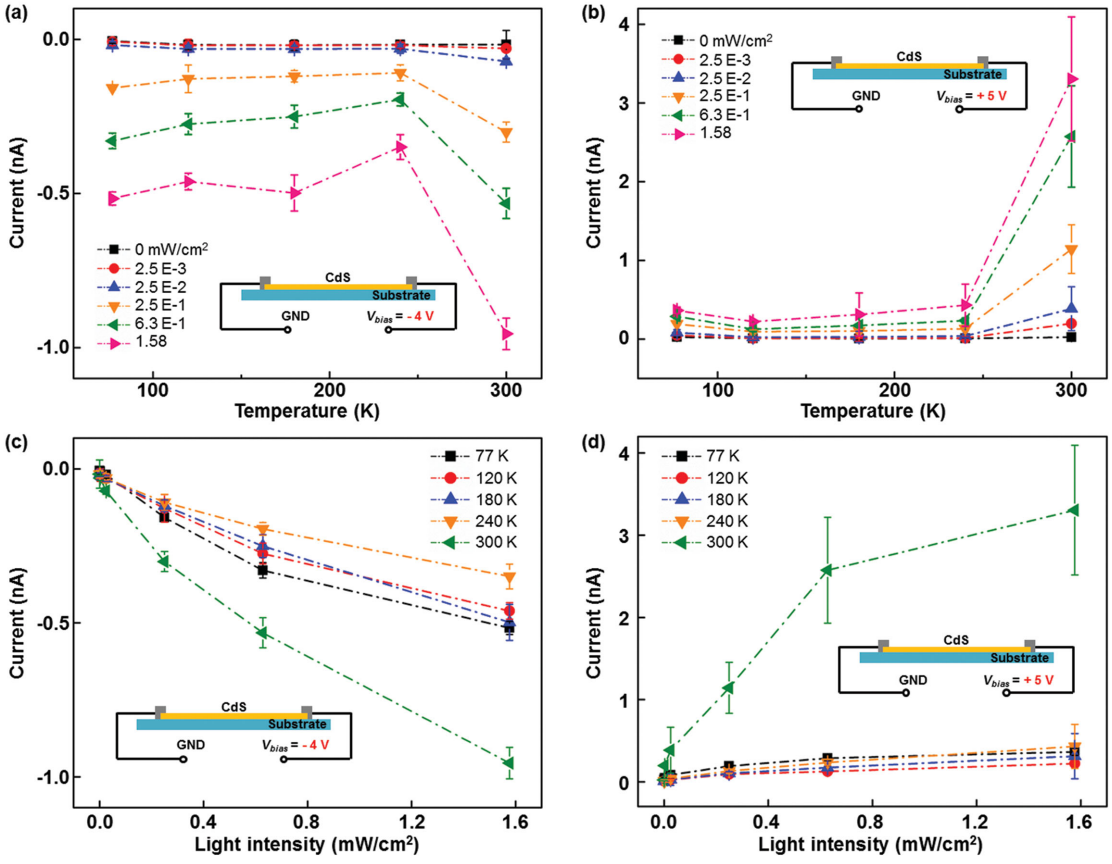

Figure 2. Current response of CdS NW devices to temperatures and illuminations. Current response of CdS NW devices to various temperatures under a series of illumination intensities and strain-free condition at a) –4 and b) +5 V biased voltage. Current response of CdS NW devices to various illuminations at different temperatures and under strain-free condition by applying a bias voltage of c) –4 and d) +5 V.

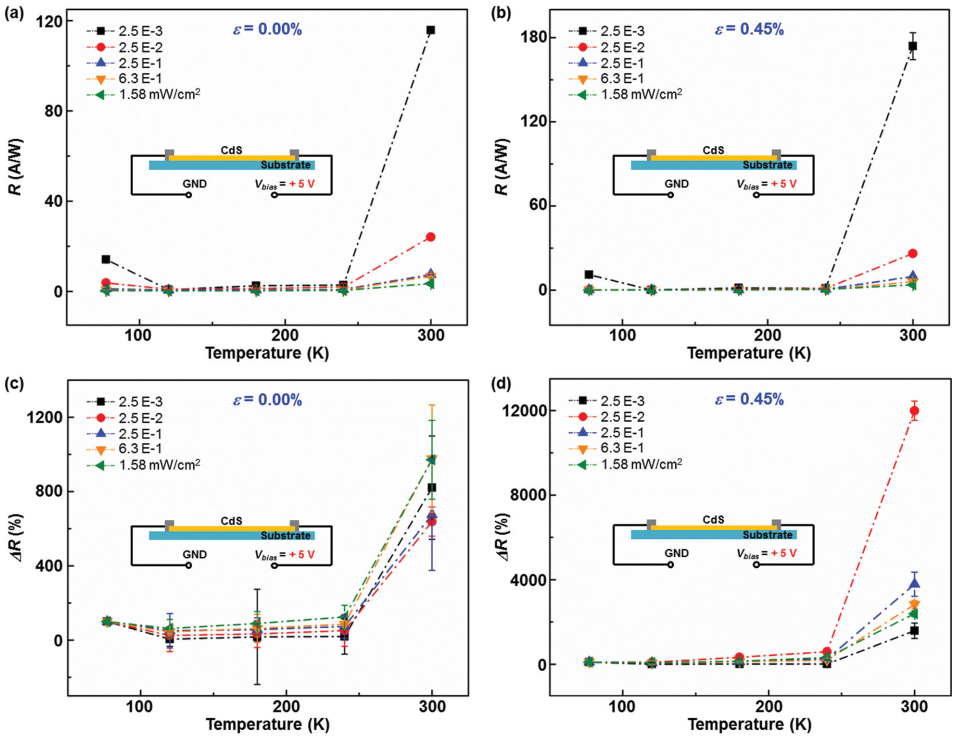

Figure 3. Temperature dependence of the photoresponsivity. Photoresponsivity of the device under various illuminations and temperatures, by applying a) 0.00% and b) 0.45% strain, biased at +5 V. Relative changes of the photoresponsivity under various illuminations and temperatures, by applying c) 0.00% and d) 0.45% strain, biased at +5 V.

2.3. Temperature Dependence of the Photoresponsivity

As a critical parameter to characterize the optoelectronic performances of CdS NW devices, the photoresponsivity R under various temperatures and illumination intensities is calculated and summarized in **Figure 3** for strain-free (Figure 3a,c) and 0.45% external strain (Figure 3b,d) conditions at a biased voltage of +5 V. The photoresponsivity[18] R is defined as

$$R = \frac{I_{\text{light,s}} - I_{\text{dark,s}}}{P_{\text{ill}}} = \frac{\eta_{\text{ext}} q}{h\nu} \cdot \Gamma_{\text{G}} \quad (1)$$

where $P_{\text{ill}} = I_{\text{ill}} \times S$ is the illumination power on the device; $I_{\text{light,s}}$ and $I_{\text{dark,s}}$ represent the photon and dark current under the corresponding external strains, respectively; Γ_{G} is the internal gain; η_{ext} is the external quantum efficiency (EQE); q is the electronic charge; h is Planck's constant; ν is the frequency of the light; I_{ill} is the excitation power density; and S is the effective area of the device. From Figure 3a,b, it is obvious that higher R is observed at room temperature under various illuminations and both strain conditions. Moreover, the highest value of 174 A/W is derived at 2.5×10^{-3} mW cm^{-2} and 300 K by applying a 0.45% external strain, indicating the enhancements on the photoresponsivity by the piezophototronic effect compared with the strain-free condition (Figure 3a). Besides, relative changes of the photoresponsivity R with respect to R_0 (corresponding photoresponsivity at 77 K) are calculated along the temperature axis under both strain-free and 0.45% strain conditions as shown in Figure 3c,d, respectively. At room temperature (300 K), the largest relative change of R is 976.7% under strain-free condition (6.3×10^{-1} mW cm^{-2}, Figure 3c), and 11 990% under 0.45% tensile strain (2.5×10^{-2} mW cm^{-2}, Figure 3d).

2.4. Temperature Dependence of the Piezophototronic Effect

2.4.1. Current Responses to Temperatures under the Piezophototronic Effect

The piezophototronic effect on the output currents of CdS NW devices is carefully studied under a series of light illuminations and straining conditions at different temperatures, ranging from 77 to 300 K, for both negative and positive biased voltages as shown in **Figure 4**. At –4 V biased voltage (Figure 4a–c), the current responses of CdS NW devices to external strains are measured under laser illuminations with power density ranging from 2.5×10^{-3} to 1.58 mW cm^{-2} at 77 K (Figure 4b), 120 K (Figure S2b, Supporting Information), 180 K (Figure S3b, Supporting Information), 240 K (Figure S4b, Supporting Information), and 300 K (Figure 4c). From these experimental results, the changes of currents present a transition from monotonously increase with increasing the externally applied tensile strains to the existence of a local maximum current at certain tensile strain as raising the measurement temperature from 77 to 300 K. Besides, the value of the tensile strain corresponding to the local maximum current decreases as increasing the temperature. Considering the fact that the piezophototronic effect is a polarized interfacial effect leading to asymmetric changes of barrier heights

Adv. Funct. Mater. **2015**,
DOI: 10.1002/adfm.201501986

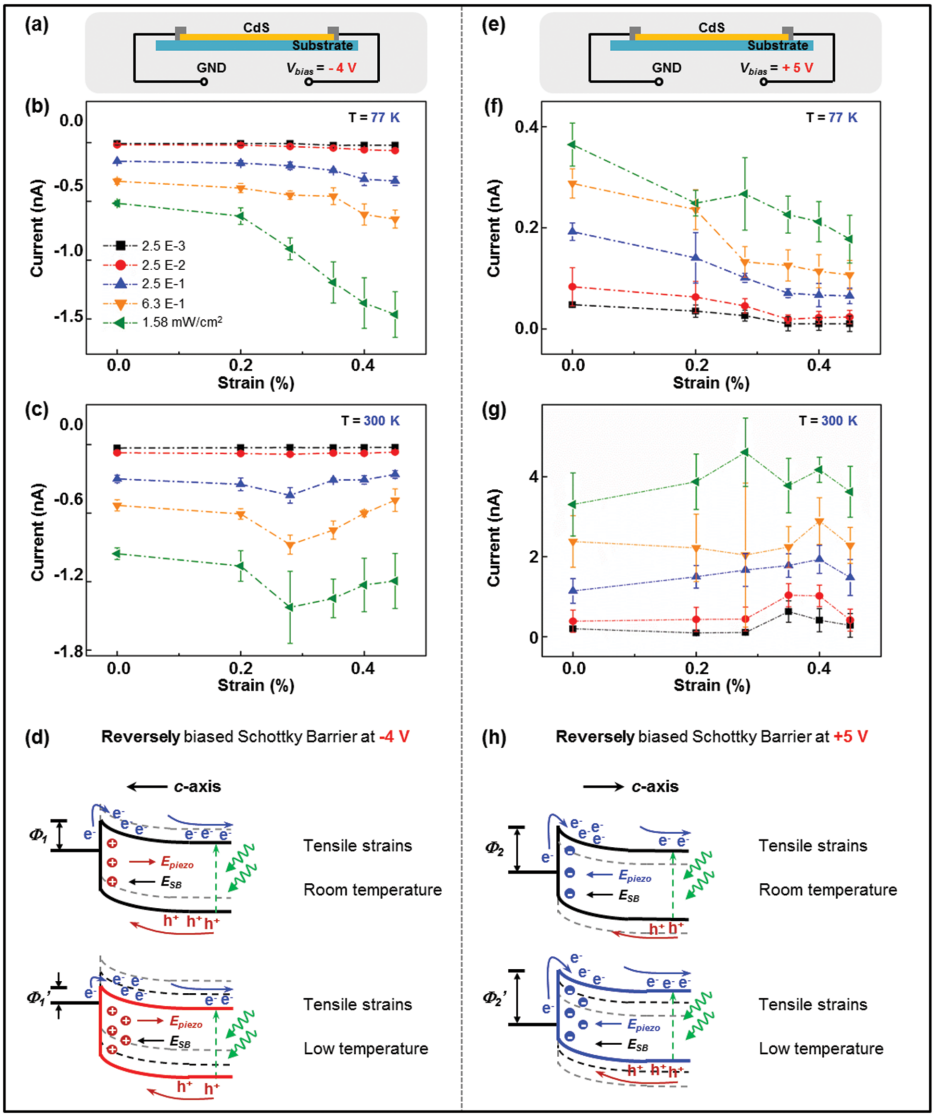

Figure 4. Temperature dependence of the piezophototronic effect and the working mechanism. a) At a bias voltage of –4 V, the current *I* versus strains curve under a series of illumination intensities at b) 77 K and c) 300 K, and d) the corresponding energy band diagrams of CdS NWs under tensile strains at room temperature (top panel) and low temperature (bottom panel). e) At a bias voltage of +5 V, the current *I* versus strains curve under a series of illumination intensities at f) 77 and g) 300 K, and h) the corresponding energy band diagrams of CdS NWs under tensile strains at room temperature (top panel) and low temperature (bottom panel). The figure legends presented in (b) are adopted for plots in (c), (f), and (g).

and the output currents at two Schottky contacts, the currents responses of CdS NW devices to external strains at +5 V biased voltage (Figure 4e–g, Figures S2d–S4d, Supporting Information) display a transition from monotonously decrease with increasing the tensile strains to the presenting of a local minimum current at certain tensile straining conditions as heating up the system from 77 to 240 K. At 300 K (Figure 4g), the currents show a local maximum value as reversing the trend of current changes.

2.4.2. Working Mechanism

Energy band diagrams of CdS NWs are schematically shown in Figure 4d,h to systematically explain the observed optoelectronic performances of CdS devices controlled by the piezophototronic effect at different temperatures. Upon straining, two of the optoelectronic processes within the CdS NW devices are tuned/controlled by the piezophototronic effect. First, the transport of the charge carriers across a reversely biased local M–S Schottky contact is dominated by the SBH, which is controlled by the effective piezoelectric polarization charges presented at the vicinity of the local interface. The density of effective piezocharges is affected by environment temperatures due to the screening effect of the local free charge carriers to the static piezoelectric charges. Second, the separation process of photogenerated charge carriers near the local contact is affected by the piezoelectric field induced by polarizations. Under a bias voltage of –4 V, positive piezoelectric polarization charges are presented at the reversely biased local Schottky contact under tensile strains (Figure 4d). Thus,

on one hand, the SBH is reduced by positive piezocharges (Figure 4d), which enhances the carrier transport across the reversely biased local Schottky barrier; on the other hand, the piezoelectric field is in an opposite direction of the current flow and hence reducing the separation efficiency of light-generated electron holes. A competition mechanism is formed between these two processes. At low temperature (Figure 4d, bottom), the separation of electron–hole pairs is almost complete with little recombination, and the screening effect to the piezoelectric charges is minimized,[19] the overall output currents are predominantly controlled by the SBH which dominates the carriers' transport across the reversely biased local Schottky contact. The more external tensile strains are applied, the lower SBH is formed. Therefore, the currents increase monotonously with increasing the tensile strains at low temperature as shown in Figure 4b. At room temperature (Figure 4d, top), the SBH at reversely biased contact is less reduced due to the enhanced screening effect by increased free electron density in CdS NWs. Moreover, the retarding of the electron–hole separation process by the piezoelectric field is becoming considerable. The combination of these two processes results in the observation of a local maximum current at room temperature as shown in Figure 4c. A transition from monotonous increase in current to local maximum current at certain straining conditions is therefore observed as raising the temperature from 77 to 300 K.

Similarly, under a bias voltage of +5 V, negative polarization charges are presented at the vicinity of the local Schottky contact under tensile strains (Figure 4h), but with reduced magnitude due to the enhanced screening effect at room temperature. In this scenario, the SBH at local interface is increased by negative piezocharges (Figure 4h) and thus hinder the carrier transport across the reversely biased local Schottky barrier. Meanwhile, the piezoelectric field is in the same direction as the current flow and improving the separation efficiency of light-generated charge carriers. There exists a competition mechanism between these two processes. Therefore, at low temperature (Figure 4h, bottom), due to the almost complete separations of electron–hole pairs,[19] the currents decrease monotonously with increasing the tensile strains as shown in Figure 4f. At room temperature (Figure 4h, top), the SBH at reversely biased M–S contact is slightly increased due to the less effective piezocharges resulted from the enhanced screening effect; while the separation efficiency of the electron–hole pairs is substantially improved by the piezoelectric field, which is in the same direction as the current flow. The combination of these two processes results in the appearance of a local minimum current as shown in Figure S3d (Supporting Information). At 300 K, the separation efficiency of photogenerated charge carriers is improved significantly by the piezoelectric field to overcome the influence of the increased SBH and start dominating the overall output currents of CdS NW devices. Therefore, a local maximum current is observed as shown in Figure 4g.

2.4.3. Piezophototronic Factor and Changes of SBH

Temperature dependence of the piezophototronic effect is further investigated by defining a physical parameter, piezophototronic factor, as the response sensitivity per unit strain: $S/\mathrm{d}\varepsilon = \mathrm{d}I/(I_0 \times \mathrm{d}\varepsilon) = (I\varepsilon_2 - I\varepsilon_1)/I\varepsilon_1(\varepsilon_2 - \varepsilon_1)$, where $I\varepsilon_2$ and $I\varepsilon_1$ correspond to the currents derived under ε_2 and ε_1 straining conditions at the same illumination intensity, respectively. The piezophototronic factors derived at –4 and +5 V biased voltages are summarized and plotted as a function of temperatures in **Figure 5**a,b, respectively. Obviously, for both biased voltages, larger piezophototronic factor is achieved at lower temperature under all the illumination intensity, with the largest value of 576.2% derived under 2.5×10^{-2} mW cm^{-2} illumination at 77 K (Figure 5a). These results clearly indicate the significantly enhanced piezophototronic effect at low temperatures, and are further confirmed by theoretically calculating the changes of SBH at the reversely biased local Schottky contact for both –4 and +5 V biased voltages, as shown in Figure 5c,d, respectively. The same M–S–M physical model as utilized for conductivity and carrier density calculations (Figure S1, Supporting Information) is applied to quantitatively simulate the transport properties of CdS NWs, and the changes of SBH are calculated through a well-developed Matlab based program PKUMSM.[17] As expected, more changes of SBH are obtained at lower temperature for both biased voltages (Figure 5c,d), which further prove the fact that the piezophototronic effect is significantly enhanced at low temperature.

2.4.4. Effective Polarization Charge Density

Considering that the changes of SBH are induced by piezoelectric polarization charges and proportional to the effective polarization charge density at the local interface/contact area,[20] more theoretical simulations are conducted to calculate the effective polarization surface charge density of CdS NWs under 1.58 mW cm^{-2} illumination. The effective surface charges at the local M–S interface under certain straining conditions are determined by[21]

$$\rho_s = \sqrt{2\varepsilon_r\varepsilon_0 kT\left[N_D\left(\frac{\Phi}{kT}\right) + n\left(\exp\left(\frac{-\Phi}{kT}\right) - 1\right)\right]} \quad (2)$$

where ρ_s is the total surface charges, N_D is the donor dopant concentration, Φ is Schottky barrier height, and n is the temperature-dependent carrier density that is equal to the ionized donor dopant concentration. Few assumptions are made here: 1) semiconductor is nondegenerate; 2) no minority carriers are presented; and 3) the ionized donor dopant concentration is a constant throughout the semiconductor. The first term in the square bracket indicates the screening against surface charges by fixed ionized dopants; the second term is the screening by mobile carriers. By assuming that all of the donors are ionized at room temperature, $N_D = n_{(T = 300\ \mathrm{K})}$. Then, the effective polarization charge density ρ_{eff} induced by mechanical strains is calculated as $\rho_{eff} = \rho_{s(\mathrm{strain}=0.45\%)} - \rho_{s(\mathrm{strain}=0\%)}$. Based on the transport properties of GaN NWs devices under various temperatures and straining conditions, the corresponding parameters, such as carrier density and SBH, are quantitatively simulated through an M–S–M model,[16,17] which connects the NW and two M–S Schottky barriers in serial. A set of current–voltage equations is obtained among these three parts. The numerical solution of this equation set is derived by using Newton

DOI: 10.1002/adfm.201501986

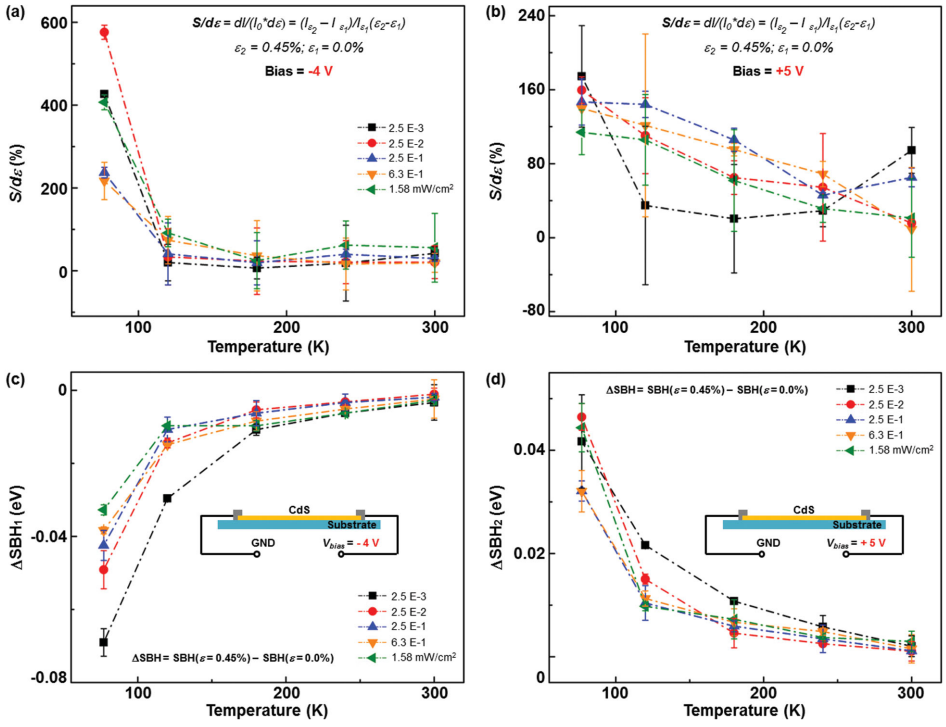

Figure 5. Temperature dependence of the piezophototronic factor at a) −4 and b) +5 V biased voltage. The piezophototronic factor is defined as the response sensitivity per unit strains: $S/d\varepsilon$. The figure legends presented in (a) are adopted for plots in (b). Calculated changes of SBH as a function of temperatures at the reversely biased Schottky contact under c) −4 V and d) +5 V between 0.45% tensile strain and strain-free condition.

method through a Matlab based program PKUMSM.[17] The calculated effective polarization charges are thus plotted as a function of temperature as shown in Figure S5 (Supporting Information). It is clear that the effective polarization charges increase as cooling down the system, leading to more changes in the SBH and significantly enhanced piezophototronic effect at lower temperature.

3. Conclusion

In conclusion, the temperature dependence of the piezophototronic effect in CdS NWs is systematically investigated by varying the temperature from 77 to 300 K. The piezophototronic effect is significantly enhanced by over 550% as cooling down the system, since the effective piezoelectric polarization charges density is increased due to the reduced screening effect by decreased mobile charge carrier density in CdS NWs at lower temperature. The conclusion is further confirmed by simulating the transport properties of CdS NW devices quantitatively through an M–S–M model at various temperatures to calculate the conductivity, mobile charge carrier density, effective polarization charge density, and the corresponding changes of SBH of CdS NWs. The fundamentals of the piezophototronic effect are explored by measuring the optoelectronic behaviors of CdS NW devices under a series of light illuminations and straining conditions at each temperature. Under mechanical strains, the corresponding energy band diagrams indicate that the piezophototronic effect dominates the transport and separation processes of charge carriers by utilizing strain-induced piezoelectric polarization charges at local interface to modulate the energy band structures of the CdS NWs. This work investigates the temperature dependence and the fundamental working mechanism of the piezophototronic effect, guiding the future design and fabrication of piezophototronic optoelectronic devices for optical communications, human-machine interfacing, health monitoring systems, and implantable surgical instruments.

4. Experimental Section

Electric Signal Measurements: A function generator (Model No. DS345, Stanford Research Systems, Inc.) and a low-noise current preamplifier (Model No. SR570, Stanford Research Systems, Inc.) were used for electrical measurements. Computer-controlled measurement software in conjunction with a GPIB controller (GPIB-USB-HS, NI 488.2) was used to collect and record the data.

Supporting Information

Supporting Information is available from the Wiley Online Library or from the author.

Acknowledgements

R.Y., X.W. and W.W. contributed equally to this work. This research was supported by U.S. Department of Energy, Office of Basic Energy Sciences

(Award No. DE-FG02-07ER46394) (personal, measurements), and MANA, National Institute For Materials Science, Japan (data analysis).

Received: May 13, 2015
Revised: June 24, 2015
Published online:

[1] Z. L. Wang, *Nano Today* **2010**, *5*, 540.
[2] Z. L. Wang, *Adv. Mater.* **2012**, *24*, 4632.
[3] a) X. D. Wang, *Am. Ceram. Soc. Bull.* **2013**, *92*, 18; b) J. Zhou, Y. D. Gu, P. Fei, W. J. Mai, Y. F. Gao, R. S. Yang, G. Bao, Z. L. Wang, *Nano Lett.* **2008**, *8*, 3035; c) W. Z. Wu, Y. G. Wei, Z. L. Wang, *Adv. Mater.* **2010**, *22*, 4711; d) W. Z. Wu, Z. L. Wang, *Nano Lett.* **2011**, *11*, 2779; e) W. Z. Wu, L. Wang, Y. L. Li, F. Zhang, L. Lin, S. M. Niu, D. Chenet, X. Zhang, Y. F. Hao, T. F. Heinz, J. Hone, Z. L. Wang, *Nature* **2014**, *514*, 470.
[4] R. M. Yu, L. Dong, C. F. Pan, S. M. Niu, H. F. Liu, W. Liu, S. Chua, D. Z. Chi, Z. L. Wang, *Adv. Mater.* **2012**, *24*, 3532.
[5] a) Y. Zhang, Z. L. Wang, *Adv. Mater.* **2012**, *24*, 4712; b) Y. Liu, S. M. Niu, Q. Yang, B. D. B. Klein, Y. S. Zhou, Z. L. Wang, *Adv. Mater.* **2014**, *26*, 7209; b) Y. Liu, Q. Yang, Y. Zhang, Z. Y. Yang, Z. L. Wang, *Adv. Mater.* **2012**, *24*, 1410.
[6] a) W. Z. Wu, C. F. Pan, Y. Zhang, X. N. Wen, Z. L. Wang, *Nano Today* **2013**, *8*, 619; b) L. Dong, S. M. Niu, C. F. Pan, R. M. Yu, Y. Zhang, Z. L. Wang, *Adv. Mater.* **2012**, *24*, 5470.
[7] a) C. F. Pan, S. M. Niu, Y. Ding, L. Dong, R. M. Yu, Y. Liu, G. Zhu, Z. L. Wang, *Nano Lett.* **2012**, *12*, 3302; b) X. N. Wen, W. Z. Wu, Z. L. Wang, *Nano Energy* **2013**, *2*, 1093.
[8] a) Q. Yang, W. H. Wang, S. Xu, Z. L. Wang, *Nano Lett.* **2011**, *11*, 4012; b) C. F. Pan, L. Dong, G. Zhu, S. M. Niu, R. M. Yu, Q. Yang, Y. Liu, Z. L. Wang, *Nat. Photonics* **2013**, *7*, 752.
[9] a) Q. Yang, X. Guo, W. H. Wang, Y. Zhang, S. Xu, D. H. Lien, Z. L. Wang, *ACS Nano* **2010**, *4*, 6285; b) Z. N. Wang, R. M. Yu, X. N. Wen, Y. Liu, C. F. Pan, W. Z. Wu, Z. L. Wang, *ACS Nano* **2014**, *8*, 12866.
[10] R. M. Yu, W. Z. Wu, C. F. Pan, Z. N. Wang, Y. Ding, Z. L. Wang, *Adv. Mater.* **2015**, *27*, 940.
[11] a) G. Santhanam, S. I. Ryu, B. M. Yu, A. Afshar, K. V. Shenoy, *Nature*, **2006**, *442*, 195; b) C. Wang, D. Hwang, Z. B. Yu, K. Takei, J. Park, T. Chen, B. W. Ma, A. Javey, *Nat. Mater.* **2013**, *12*, 899; c) B. C. K. Tee, C. Wang, R. Allen, Z. N. Bao, *Nat. Nanotechnol.* **2012**, *7*, 825; d) B. Z. Tian, J. Liu, T. Dvir, L. H. Jin, J. H. Tsui, Q. Qing, Z. G. Suo, R. Langer, D. S. Kohane, C. M. Lieber, *Nat. Mater.* **2012**, *11*, 986; e) W. Z. Wu, X. N. Wen, Z. L. Wang, *Science* **2013**, *340*, 952.
[12] F. X. Gu, Z. Y. Yang, H. K. Yu, J. Y. Xu, P. Wang, L. M. Tong, A. L. Pan, *J. Am. Chem. Soc.* **2011**, *133*, 2037.
[13] Y. F. Lin, J. Song, Y. Ding, S. Y. Lu, Z. L. Wang, *Adv. Mater.* **2008**, *20*, 3127.
[14] Y. F. Hu, B. D. B. Klein, Y. J. Su, S. M. Niu, Y. Liu, Z. L. Wang, *Nano Lett.* **2013**, *13*, 5026.
[15] R. S. Yang, Y. Qin, L. M. Dai, Z. L. Wang, *Nat. Nanotechnol.* **2009**, *4*, 34.
[16] Z. Y. Zhang, K. Yao, Y. Liu, C. H. Jin, X. L. Liang, Q. Chen, L. M. Peng, *Adv. Funct. Mater.* **2007**, *17*, 2478.
[17] Y. Liu, Z. Y. Zhang, Y. F. Hu, C. H. Jin, L. M. Peng, *J. Nanosci. Nanotechnol.* **2008**, *8*, 252.
[18] G. Konstantatos, E. H. Sargent, *Nat. Nanotechnol.* **2010**, *5*, 391.
[19] M. H. Hecht, *Phys. Rev. B* **1990**, *41*, 7918.
[20] Y. Zhang, Y. Liu, Z. L. Wang, *Adv. Mater.* **2011**, *23*, 3004.
[21] a) W. Mönch, *Semiconductor Surface and Interfaces*, Springer, Berlin **1993**; b) S. Chevtchenko, X. Ni, Q. Fan, A. A. Baski, H. Morkoc, *Appl. Phys. Lett.* **2006**, *88*, 122104.